ISSN 1541-308X, Physics of Wave Phenomena, 2019, Vol. 27, No. 4, pp. 313–319. © Allerton Press, Inc., 2019.

UNDERWATER ACOUSTICS

Intense Internal Waves and Their Manifestation in the Interference Patterns of Received Signals on Oceanic Shelf. Part II

M. Badiey[1*], V. M. Kuz'kin[2], G. A. Lyakhov[2***], S. A. Pereselkov[2,3****], D. Yu. Prosovetskiy[3*****], and S. A. Tkachenko[3******]**

[1] *University of Delaware, Newark, DE 19716, USA*

[2] *Prokhorov General Physics Institute of the Russian Academy of Sciences, ul. Vavilova 38, Moscow, 119991 Russia*

[3] *Voronezh State University, Universitetskaya pl. 1, Voronezh, 394006 Russia*

Received December 25, 2018; in final form, December 25, 2018; accepted December 30, 2018

Abstract—Data of the SWARM-95 experiment, where intense internal waves on a stationary path led to coupling of acoustic source field modes, have been processed. The spectral-density localization domains, which are due to unperturbed and perturbed fields, are obtained using a double Fourier transform of interference pattern on a hologram. The interference patterns of these fields have been reconstructed by filtering these regions and applying double inverse Fourier transforms to them, which made it possible to reconstruct the unperturbed-waveguide transfer function and the time variability of the medium. The velocity of intense internal waves is estimated based on the recorded perturbed-field hologram.

DOI: 10.3103/S1541308X19040125

1. INTRODUCTION

The SWARM-95 experiment was carried out on the New Jersey coast [1–4]. Stationary acoustic paths made angles $\beta_1 = 5°$ (the first path) and $\beta_2 = 39°$ (the second path) with the front of intense internal waves (IIWs); the angle between the path directions was $\alpha = 34°$ (Fig. 1). The speed-of-sound depth profile is shown in Fig. 2. Along the first (14.98-km-long) and second (17.95-km-long) paths, the depth varied within 71–73 and 70–88 m, respectively. The IIW amplitude reached ≈10 m, the propagation velocity was ≈0.65 m s^{-1}, the time scale of variability was ≈10 min [5]. An airgun source, located at a depth of 12 m, emitted a 0.2-s pulse every minute; the pulse spectrum is shown in Fig. 2 [6]. The signal from a single hydrophone of a vertical linear antenna, located at a depth of 36 m, is considered here.

On the first and second paths, the IIWs caused horizontal refraction of sound waves and coupling of source field modes, respectively. The horizontal refraction and mode coupling are two limiting cases of the IIW influence on acoustic fields. The reconstructed interference patterns of the unperturbed and perturbed (scattered from refractive-index inhomogeneities) fields on the first path, obtained using holographic sound-source localization [7], were presented in [6]. Here, the dependence of the squared modulus of sound pressure on time and frequency, caused by the interference of source-field normal modes, is considered to be an interference pattern, and the double

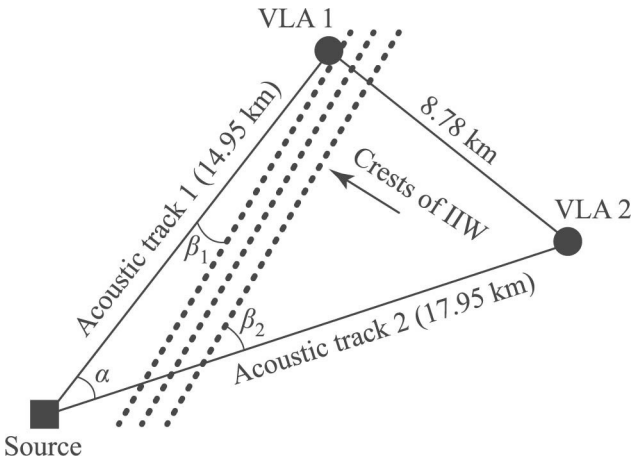

Fig. 1. Schematic of the experiment [2]. The vertical linear antennas of the first and second paths are denoted as VLA 1 and VLA 2, respectively.

*E-mail: badiey@udel.edu
**E-mail: kumiov@yandex.ru
***E-mail: gen.lyakhov@gmail.com
****E-mail: pereselkov@yandex.ru
*****E-mail: prosovetskiy@gmail.com
******E-mail: sega-tk@mail.ru

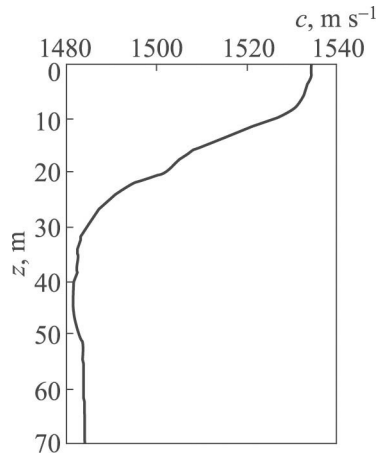

Fig. 2. Unperturbed speed-of-sound profile [5].

Fourier transform of the interference pattern is referred to as a hologram.

Following [6], the interference patterns of the unperturbed and scattered fields on the second path were reconstructed. Based on the holograms obtained, the IIW propagation velocity was estimated and the unperturbed-waveguide transfer function and time variability of the medium were reconstructed.

2. PRINCIPLE OF INTERFERENCE PATTERN RECONSTRUCTION

The variations in the ocean-medium refractive index, being caused by a hydrodynamic perturbation, initiate changes in the horizontal wave numbers (and, in general, mode amplitudes) with respect to the unperturbed values. This leads to the following: the resulting interference pattern, which is determined by the difference in the horizontal wave numbers, is a linear superposition of two independent interference patterns, generated by unperturbed and scattered fields. A double Fourier transform of an interference pattern (in view of linearity) creates two independent localized domains in the form of focal spots on a hologram. The first domain, related to the unperturbed field, is concentrated mainly along the time axis, whereas the second domain, which is due to the hydrodynamic perturbation, is concentrated along the frequency axis. The holograms of these fields can be separated by filtering the domains. Their interference patterns can be reconstructed by applying a double inverse Fourier transform to them. In the former and latter cases, the interference pattern is formed by the interference of modes of unperturbed and perturbed media, respectively. With a known source spectrum, one can reconstruct the unperturbed-waveguide transfer function and examine the time variability of the medium.

3. PROCESSING RESULTS

The data processing on the first path was performed with the same single-receiver depth and frequency ranges as in [6]; this approach (under the same receiving conditions) makes it possible to estimate the influence of the path position with respect to the IIW front on the operation of the holographic method [7], when the latter is used to reconstruct the interference patterns of unperturbed and perturbed fields.

Figure 3 shows the initial interference patterns and holograms in the presence of IIWs for several frequency ranges. To increase the contrast and resolution, the mean values are cut in the interference patterns. The modulus of normalized hologram in the three-dimensional image is indicated as $|\widehat{F}|$. At low frequencies, when the scattering from inhomogeneities is insignificant, vertical localized fringes, related to the unperturbed waveguide, dominate in the interference pattern. The scattering effects are enhanced with an increase in frequency, as a result of which the contribution from the horizontal localized fringes increases and the interference pattern becomes more complicated (Figs. 3(a), 3(d), 3(g), and 3(j)). The focal spots of holograms are located mainly on the time and frequency axes (Figs. 3(b), 3(c), 3(e), 3(f), 3(h), 3(i), 3(k), and 3(l)). The spectral density beyond these spots is significantly suppressed. Superposition of focal spots with maximum intensity is practically absent, due to which one can reconstruct the transfer function and observe the time variability of the medium.

Filtering of the focal spots located on the frequency axis and application of double inverse Fourier transform to them is shown in Fig. 4. The spectral densities are barely along the time axis; therefore, the reconstructed interference patterns in the form of horizontal localized fringes can be assumed to be caused by a hydrodynamic perturbation. An increase in frequency does not lead to ripple effect in the interference patterns (stronger manifestation of the small-scale perturbation structure). The IIW propagation velocity w can be estimated from the scattered-field hologram ([7], formula (29)). According to [2], the differences in the horizontal wave numbers $h_{mn} = h_m - h_n$ for the neighboring mode numbers at a frequency of $f_0 = 64$ Hz are $h_{12} = 0.00928\,\mathrm{m}^{-1}$, $h_{23} = 0.0144\,\mathrm{m}^{-1}$, $h_{34} = 0.0113\,\mathrm{m}^{-1}$, and $h_{45} = 0.0158\,\mathrm{m}^{-1}$. The principal maximum in the hologram (Figs. 4(a) and 4(b)) is located at $\nu_1 = 0.0015$ Hz. As a result, we have $w = 0.74\,\mathrm{m\,s}^{-1}$, a value close to the experimental estimate: $0.65\,\mathrm{m\,s}^{-1}$.

The filtering of the spectral densities of the holograms concentrated near the time axis and their normalized Fourier transform are shown in Fig. 5. The

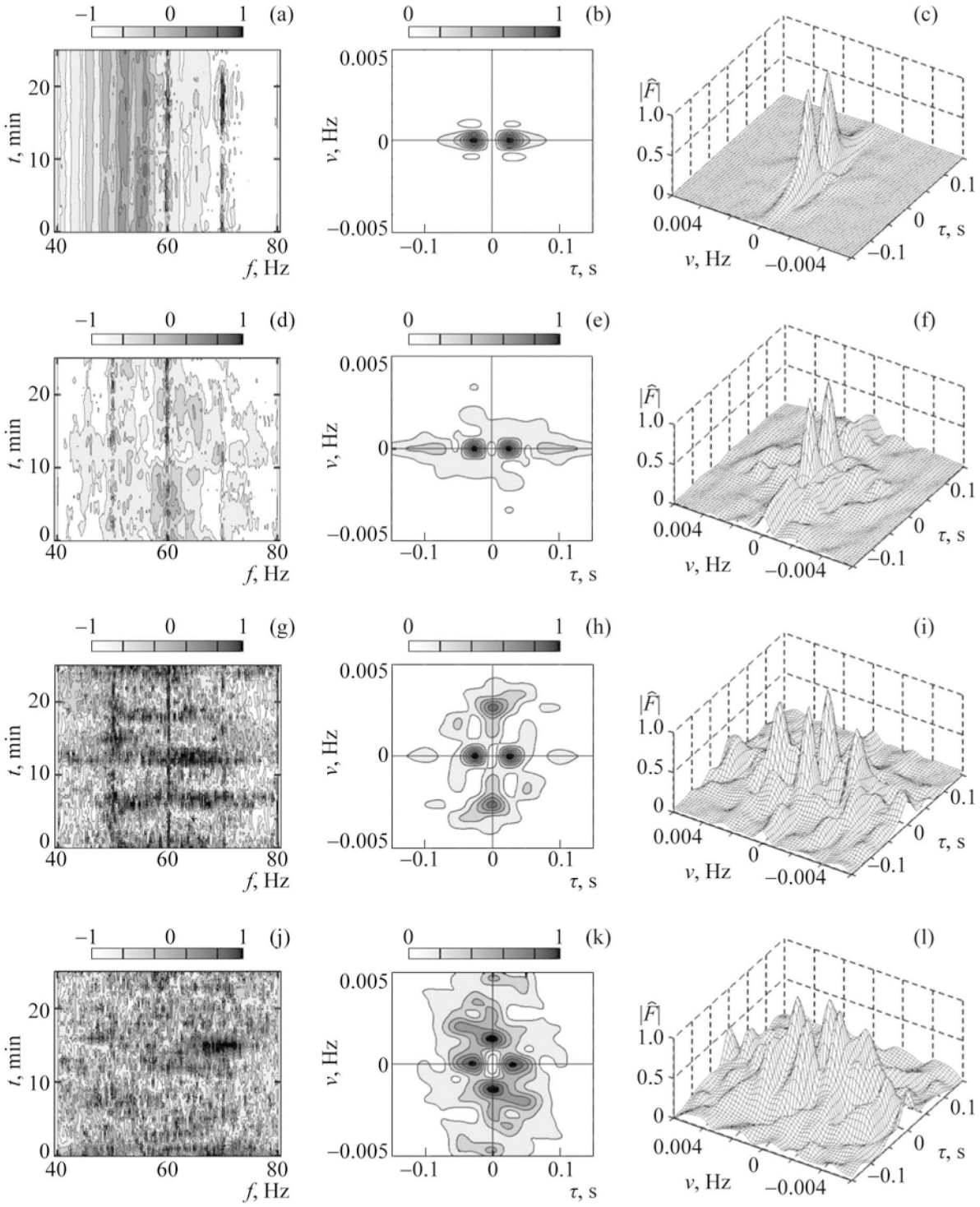

Fig. 3. Normalized (a, d, g, j) interference patterns and (b, c, e, f, h, i, k, l) holograms for various frequency ranges in the presence of IIWs. The bandwidths are 40 to 80 (a–c), 180 to 220 (d–f), 380 to 420 (g–i), and 580 to 620 Hz (j–l).

interference patterns look like sets of vertical localized fringes; hence, their occurrence can be caused by the interference of unperturbed-field modes. With an increase in frequency, the number of sound-field modes increases, and the small-scale variability of the interference pattern is intensified.

Figure 6 shows the normalized time interference patterns at frequencies of 60 (a), 200 (b), 400 (c), and 600 Hz (d), which are vertical cuts of the reconstructed two-dimensional IIW-induced interference patterns (Figs. 4(c), 4(f), 4(i), and 4(l)). The asynchronous behavior of time variability at various fre-

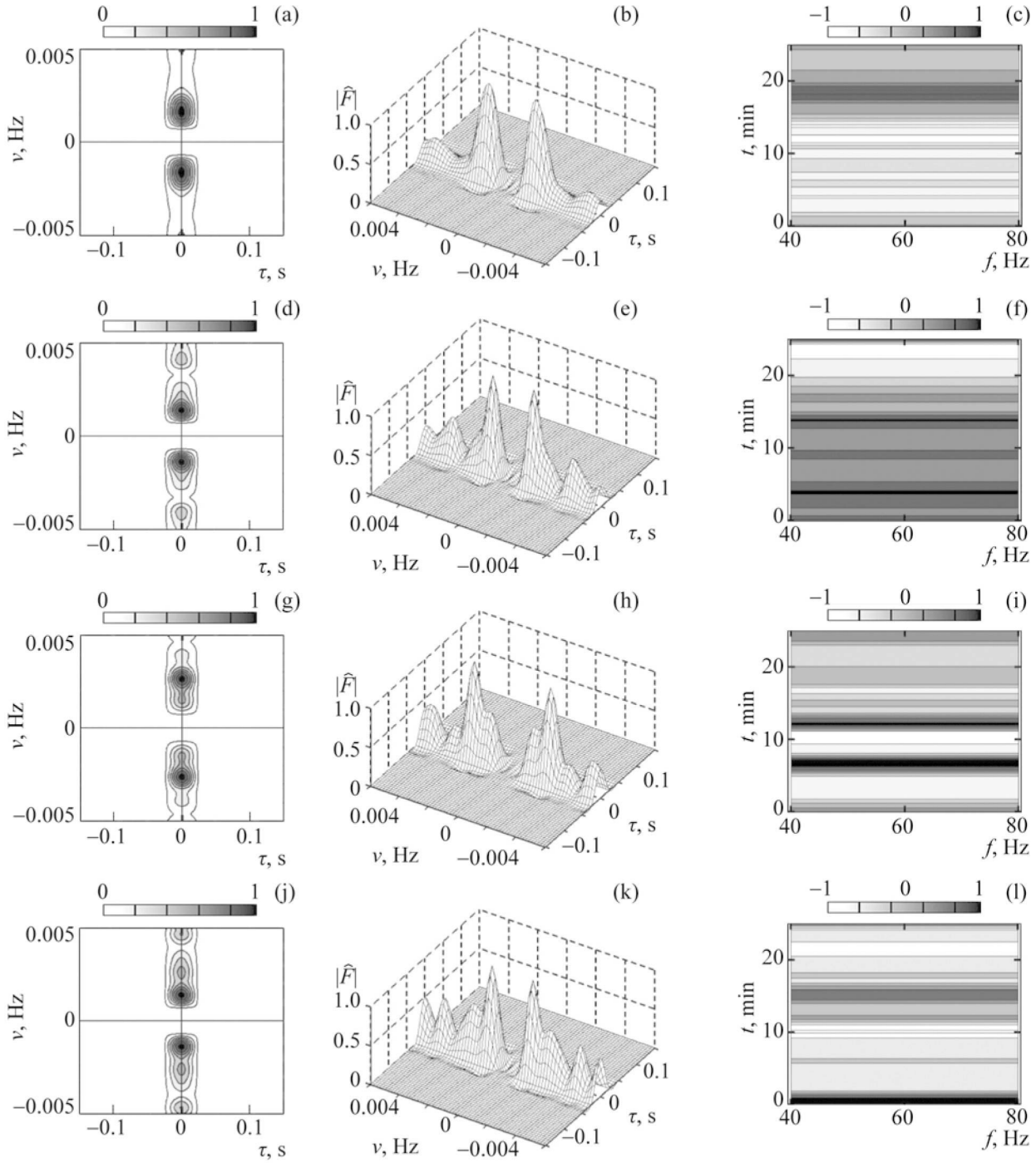

Fig. 4. (a, b, d, e, g, h, j, k) Filtering of the spectral density of a hologram localized near the frequency axis and (c, f, i, l) reconstruction of interference patterns for various frequency ranges.

quencies is related to the dependence of the perturbation of horizontal wave numbers on their unperturbed values, a fact suggesting their frequency dependence.

The squared modulus of the waveguide transfer function $|G(f)|^2$ is

$$|G(f)|^2 = \frac{|I(f)|}{|S(f)|^2}, \qquad (1)$$

where $S(f)$ is the emitted-signal spectrum and $I(f)$ is the horizontal cross section of the reconstructed interference pattern of unperturbed waveguide (Figs. 5(c), 5(f), 5(i), and 5(l)).

Figure 7 shows the frequency dependence of (1). As one would expect, the frequency scale Λ of the waveguide transfer-function oscillations decreases

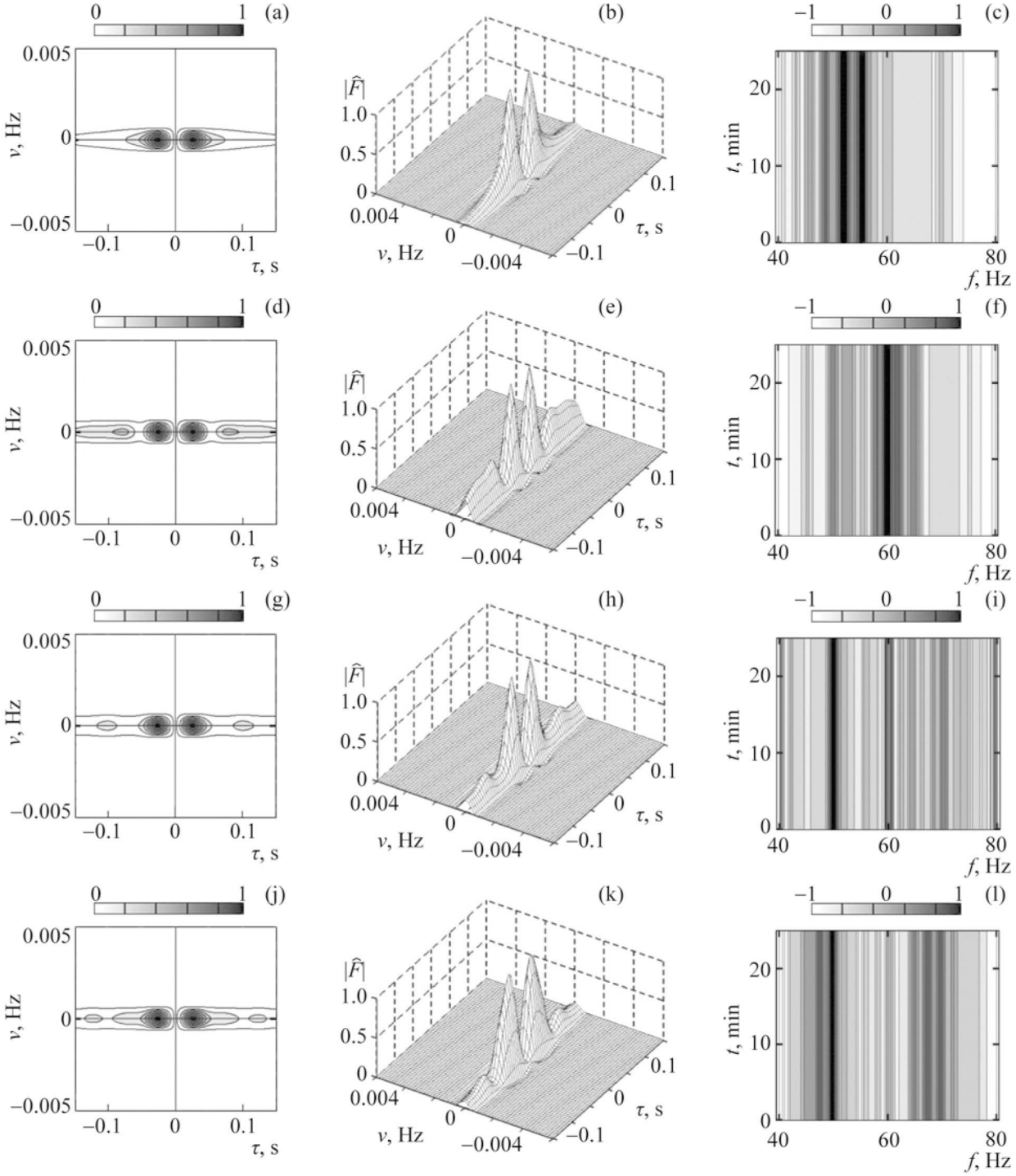

Fig. 5. (a, b, d, e, g, h, j, k) Filtering of the spectral density of a hologram localized near the time axis and (c, f, i, l) reconstruction of interference patterns for various frequency ranges.

with an increase in frequency. In the frequency ranges of 40 to 80 (Fig. 7(a)), 180 to 220 (Fig. 7(b)), 380 to 420 (Fig. 7(c)), and 580 to 620 Hz (Fig. 7(d)), $\Lambda = 3.2$, 2.8, 1.9, and 1.7 Hz, respectively.

A change in frequency leads to a redistribution of the spectral densities of the holograms formed in the absence and the presence of perturbation (see Fig. 3). This intensity redistribution can be described by the ratio

$$g(f) = |F\max(\nu, f)|/|F\max(\tau, f)|, \qquad (2)$$

where $|F\max(\nu, f)|$ and $|F\max(\tau, f)|$ are the maxima of the hologram focal spots, corresponding to the scattered and unperturbed fields, respectively.

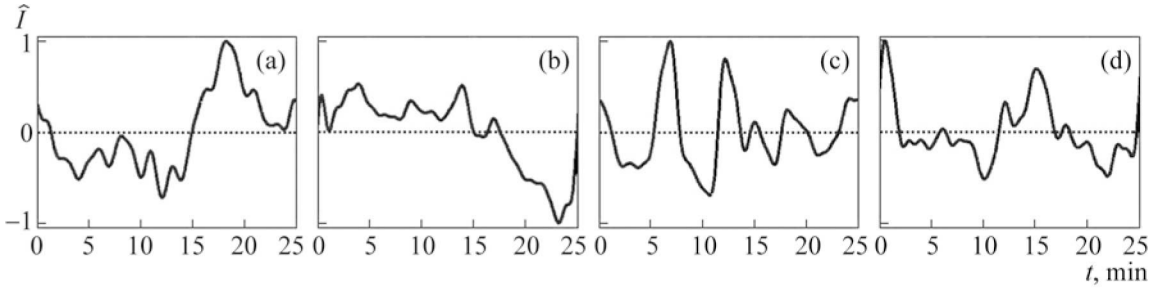

Fig. 6. Cut of the reconstructed interference patterns of scattered field at frequencies of 60 (a), 200 (b), 400 (c), and 600 Hz (d).

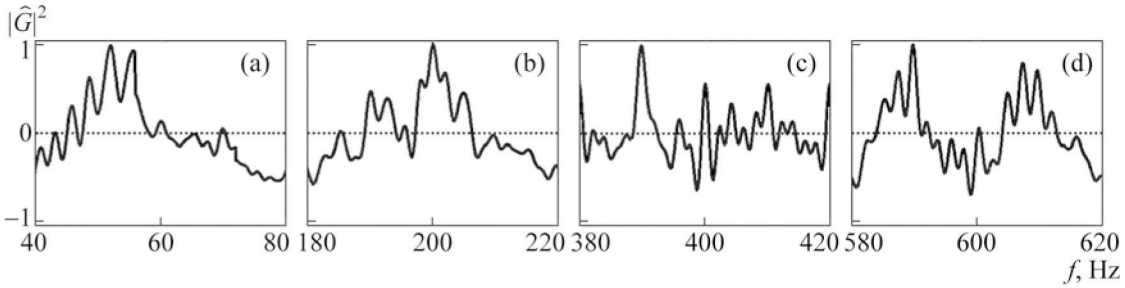

Fig. 7. Reconstructed squared modulus of the unperturbed-waveguide transfer function.

The plot of function (2) with a resolution of 5 Hz is shown in Fig. 8. The frequency scale of variability is ≈42 Hz. The dependence is resonant, with the envelope peaking at a frequency of ≈370 Hz. The reason is that the perturbation of the horizontal wave numbers depends resonantly on the frequency, and the wave numbers are peaking at the frequency in the vicinity of which the field-forming modes are maximally overlapped with the thermocline [5]. In the experiment, the thermocline was located at a depth $10 < z < 35$ m (see Fig. 2).

As one would expect, the position of the maximum of function $g(f)$ barely changed in comparison with the first path ([6], Fig. 7), the maximum value decreased by a factor of 1.6, and the characteristic frequency scale of variability increased by a factor of 1.2. The latter circumstance is explained by the geometric factor: the frequency scales $\Lambda_{1,2}$ of variability $g(f)$ on the first and second paths are linked by the relation $\Lambda_1 = \Lambda_2 \cos\alpha$. Assuming that $\Lambda_1 = 30$ Hz [6] and $\alpha = 34°$, we obtain $\Lambda_2/\Lambda_1 = 1.4$, which is in agreement with the experimental estimate.

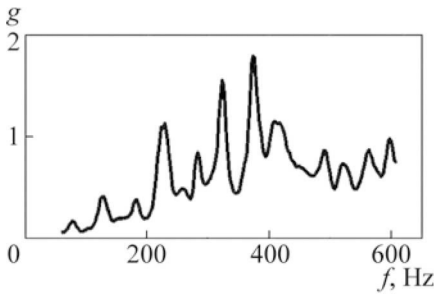

Fig. 8. Frequency dependence of the ratio of the spectral maxima of focal spots in the presence and in the absence of IIWs.

4. CONCLUSIONS

We used the holographic method to experimentally demonstrate the reconstruction of the unperturbed-waveguide transfer function and the possibility of observing the time variability of the medium under the conditions of mode coupling (caused by the IIW manifestation) for the source acoustic field. The holographic method is based on recording the initial Fourier hologram, formed by unperturbed and scattered fields. The hologram is a set of separated localized domains of spectral densities, related to the absence or presence of perturbation. The application of double inverse Fourier transform to these domains made it possible to obtain the interference patterns of unperturbed and scattered fields. The perturbation propagation velocity was estimated based on the scattered-field hologram.

Having generalized the results obtained on two paths, we can suggest that they are also applicable to other hydrodynamic perturbations of oceanic shelf (such as background internal waves, surface roughness, and tidal oscillations). Thus, the holographic method makes it possible to comprehend anew the phenomena in ocean acoustics where the wave interference caused by a broadband signal is critical.

FUNDING

Researches of S.A. Tkachenko was supported by the Russian Foundation for Basic Research (Project 19-08-00941), S.A. Pereselkov was supported by Ministry of Education and Science of the Russian Federation (Project 14.Z50.31.0037), D.Yu. Prosovietskiy was supported by grant of the President of the Russian Federation (Project MK-933.2019.8)

REFERENCES

1. J.R. Apel, M. Badiey, C.-S. Chiu, S. Finette, R.H. Headrick, J. Kemp, J.F. Lynch, A.E. Newhall, M.H. Orr, B.H. Pasewark, D. Tielburger, A. Turgut, K. Von der Heydt, and S.N. Wolf, "An Overview of the SWARM 1995 Shallow-Water Internal Wave Acoustic Scattering Experiment," IEEE J. Ocean. Eng. **22**, 465 (1997).
2. S.D. Frank, M. Badiey, J. Lynch, and W.L. Siegmann, "Analysis and Modeling of Broadband Airgum Data Influenced by Nonlinear Internal Waves," J. Acoust. Soc. Am. **116**(6), 3404 (2004).
3. M. Badiey, Y. Mu, J.F. Lynch, J.R. Apel, and A.N. Wolf, "Temporal and Azimuthal Dependence of Sound Propagation in Shallow Water with Internal Waves," IEEE J. Ocean. Eng. **27**(1), 117(2002).
4. S.D. Frank, M. Badiey, J.F. Lynch, and W.L. Siegmann, "Experimental Evidence of Three-Dimensional Acoustic Propagation Caused by Nonlinear Internal Waves," J. Acoust. Soc. Am. **118**(2), 723 (2005).
5. M. Badiey, B.G. Katsnelson, J.F. Lynch, S.A. Pereselkov, and W.L. Siegmann, "Measurement and Modeling of Three-Dimensional Sound Intensity Variations Due to Shallow-Water Internal Waves," J. Acoust. Soc. Am. **117**(2), 613 (2005).
6. V.M. Kuz'kin, S.A. Pereselkov, V.G. Zvyagin, A.Yu. Malykhin, and D.Yu. Prosovetskiy, "Intense Internal Waves and Their Manifestation in Interference Patters of Received Signals on Oceanic Shelf," Phys. Wave Phenom. **26**(2), 160 (2018) [DOI: 10.3103/S1541308X18020103].
7. G.N. Kuznetsov, V.M. Kuz'kin, and S.A. Pereselkov, "Spectrogram and Localization of a Sound Source in Shallow Water," Acoust. Phys. **63**(4), 449 (2017) [DOI: 10.1134/S1063771017040078].